Atmos. Meas. Tech. Discuss., 7, 6917–6969, 2014
www.atmos-meas-tech-discuss.net/7/6917/2014/
doi:10.5194/amtd-7-6917-2014

Atmospheric Measurement Techniques Discussions

Empirical validation and proof of added value of MUSICA's tropospheric δD remote sensing products

M. Schneider[1], Y. González[2], C. Dyroff[1], E. Christner[1], A. Wiegele[1], S. Barthlott[1], O. E. García[2], E. Sepúlveda[2], F. Hase[1], J. Andrey[3,*], T. Blumenstock[1], C. Guirado[2], R. Ramos[2], and S. Rodríguez[2]

[1]Institute for Meteorology and Climate Research (IMK-ASF), Karlsruhe Institute of Technology, Karlsruhe, Germany
[2]Izaña Atmospheric Research Center, Agencia Estatal de Meteorología (AEMET), Spain
[3]Area de Investigación e Instrumentación Atmosférica, INTA, Torrejón de Ardoz, Spain
[*]now at: CNRM-GAME, Météo France and CNRS, Toulouse, France

Received: 2 March 2014 – Accepted: 22 May 2014 – Published: 14 July 2014

Correspondence to: M. Schneider (matthias.schneider@kit.edu)

Published by Copernicus Publications on behalf of the European Geosciences Union.

Abstract

The project MUSICA (MUlti-platform remote Sensing of Isotopologues for investigating the Cycle of Atmospheric water) integrates tropospheric water vapour isototopologue remote sensing and in-situ observations. This paper presents a first empirical validation of MUSICA's H_2O and δD remote sensing products (generated from ground-based FTIR, Fourier Transform InfraRed, spectrometer and space-based IASI, Infrared Atmospheric Sounding Interferometer, observation). As reference we use well calibrated in-situ measurements made aboard an aircraft (between 200 and 6800 m a.s.l.) by the dedicated ISOWAT instrument and on the island of Tenerife at two different altitudes (at Izaña, 2370 m a.s.l., and at Teide, 3550 m a.s.l.) by two commercial Picarro L2120-i water isotopologue analysers.

The comparison to the ISOWAT profile measurements shows that the remote sensors can well capture the variations in the water vapour isotopologues and the scatter with respect to the in-situ references suggests a δD random uncertainty for the FTIR product of much better than 45 ‰ in the lower troposphere and of about 15 ‰ for the middle troposphere. For the middle tropospheric IASI δD product the study suggests a respective uncertainty of about 15 ‰. In addition, we find indications for a positive δD bias in the remote sensing products.

The δD data are scientifically interesting only if they add information to the H_2O observations. We are able to qualitatively demonstrate the added value of the MUSICA δD remote sensing data by comparing δD-vs.-H_2O curves. First, we show that the added value of δD as seen in the Picarro data is similarly seen in FTIR data measured in coincidence. Second, we document that the δD-vs.-H_2O curves obtained from the different in-situ and remote sensing data sets (ISOWAT, Picarro at Izaña and Teide, FTIR, and IASI) consistently identify two different moisture transport pathways to the subtropical north eastern Atlantic free troposphere.

AMTD
7, 6917–6969, 2014

1 Introduction

The water cycle (continuous evaporation, transport, and condensation of water) is closely linked to the global energy and radiation budgets and has thus fundamental importance for climate on global as well as regional scales. Understanding the different, strongly coupled, and often competing processes that comprise the tropospheric water cycle is of prime importance for reliable climate projections. Since different water cycle processes differently affect the isotopic composition of atmospheric water, respective measurements are potentially very useful for tropospheric water cycle research. For instance, they can help to investigate cloud processes (Webster and Heymsfield, 2003; Schmidt et al., 2005), rain recycling and evapotranspiration (Worden et al., 2007), or the processes that control upper tropospheric humidity (Risi et al., 2012).

In the following, we express $H_2{}^{16}O$ and $HD^{16}O$ as H_2O and HDO, respectively; and $\frac{HD^{16}O}{H_2{}^{16}O}$ in the δ-notation (with the Vienna standard mean ocean water, VSMOW = 3.1152×10^{-4}, Craig, 1961):

$$\delta D = \frac{HD^{16}O/H_2{}^{16}O}{VSMOW} - 1 \quad (1)$$

Tropospheric water isotopologue data obtained by space- and ground-based remote sensing techniques are particularly useful, since they can be produced continuously and at global scale. Schneider et al. (2012) present tropospheric H_2O and δD remotely-sensed from the ground at ten globally distributed FTIR (Fourier-Transform Infrared) stations of the NDACC (Network for the Detection of Atmospheric Composition Change, http://www.acd.ucar.edu/irwg/). Space-based remote sensing observations of tropospheric δD are possible by thermal nadir sensors (Worden et al., 2006; Schneider and Hase, 2011; Lacour et al., 2012) and sensors detecting reflected solar light in the near infrared (Frankenberg et al., 2009, 2013; Boesch et al., 2013).

While there have been efforts for theoretically assessing the quality of the remotely-sensed δD products (e.g. Schneider et al., 2006b, 2012; Worden et al., 2006;

AMTD
7, 6917–6969, 2014

Schneider and Hase, 2011; Lacour et al., 2012; Boesch et al., 2013), so far no really convincing empirical quality assessment has been presented. The few existing studies consist of very few indirect comparisons (Worden et al., 2011) or use a δD reference that itself is not comprehensively validated (Schneider and Hase, 2011; Boesch et al., 2013). This situation is rather unsatisfactory: since δD remote sensing measurements are very difficult and the nature of the data is very complex, there is urgent need to support the theoretical quality assessment studies by convincing empirical validation exercises.

In this context the main objective of our paper is the empirical validation of tropospheric water vapour isotopologue remote sensing products. To do so we use tropospheric δD reference data obtained by continuously calibrated in-situ instruments. The study is made for the Izaña observatory and the surroundings of the island of Tenerife, where tropospheric water isotopologues have been measured in coincidence from different platforms and by different techniques: (1) ground-based FTIR remote sensing within NDACC, (2) space-based remote sensing with the sensor IASI aboard METOP, (3) continuous in-situ measurements with commercial Picarro instruments from ground at two different altitudes, and (4) aircraft in-situ measurements with the dedicated ISOWAT instrument. All these data have been generated within the project MUSICA (www.imk-asf.kit.edu/english/musica). The Izaña observatory and the surroundings of Tenerife comprise the principle water vapour isotopologue reference area of MUSICA and allow an empirical validation with dedicated aircraft campaign data as well as with long-term data sets.

Section 2 briefly presents the in-situ observations that we use as reference. In Sect. 3 we briefly describe the investigated ground- and space-based remote sensing data. In Sects. 4 and 5 the inter-comparisons are shown and discussed. Section 6 resumes the study.

AMTD
7, 6917–6969, 2014

2 The in-situ reference observations

Compared to the remote sensing measurements, the in-situ techniques have the great advantage that they can be continuously calibrated against an isotopologue standard. In the following we briefly describe the in-situ instruments as operated in the Tenerife area.

2.1 Aircraft-based ISOWAT

The ISOWAT instrument is a tunable diode laser spectrometer specifically designed for the use aboard research aircraft (Dyroff et al., 2010). The first prototype has been successfully used within the project CARIBIC (Civil Aircraft for the Regular Investigation of the atmosphere Based on an Instrument Container, http://www.caribic-atmospheric.com/). For the validation campaign, a second prototype of ISOWAT was installed aboard a CASA C-212 aircraft of INTA (Instituto Nacional de Técnica Aeroéspacial, http://www.inta.es/).

ISOWAT measures δD in water vapour by means of laser-absorption spectroscopy. Ambient air is extracted from the atmosphere and is pumped through a multi-reflection measurement cell. The beam of a diode laser is guided into the cell where it is reflected back and forth between two mirrors to form an optical path of 32 m. The emission wavelength of the laser is continuously tuned across individually resolved absorption lines of the $H_2{}^{16}O$ and $HD^{16}O$ isotopologues at a frequency of 10 Hz. Absorption spectra are averaged over 1 s, which defines the maximum temporal resolution of the measurements.

During the campaign ISOWAT was calibrated before and after each flight performing measurements of a known isotope standard. The standard was provided by a custom designed bubbler system that was used to humidify dry synthetic air to δD of about −130 ‰ at humidity ranging from about 200 ppmv to > 25 000 ppmv. One of the key strengths of ISOWAT is its in-flight calibration. While substantial calibration measurements were performed on the ground, we perform in-flight calibrations in order to

AMTD
7, 6917–6969, 2014

confirm the instrumental performance during the flight. The in-flight calibration source provided a known isotope standard at a humidity of 3000–5000 ppmv. Thereby, ambient air was first dried (< 5 ppmv) in a cartridge containing molecular sieve. The dry air was then humidified in a small temperature-stabilised bubbler system. Calibrations were performed 2–5 times per flight at varying altitudes in order to check the performance of ISOWAT under all environmental conditions. Using the ground-based and in-flight calibration measurements performed during the MUSICA campaign we were able to determine the accuracy of ISOWAT. For the majority of conditions encountered, ISOWAT provided profile measurements with an uncertainty for δD of about 10 ‰. Below 2000 ppmv the uncertainty increases and can exceed 35 ‰ for a humidity below 500 ppmv.

The ISOWAT humidity data are calibrated against a commercial hygrometer. We estimate a precision and accuracy of about 4 %.

ISOWAT measures the isotopologues with a temporal resolution of 1 s. This translates to a horizontal spatial resolution of about 80 m depending on the aircraft velocity. During the MUSICA campaign, profile flights consisted in a relatively fast ascent followed by a slower descent with intermediate level flights at certain selected altitudes and we achieved an average vertical resolution of about 1.2 m. The good temporal resolution of ISOWAT allows observing the rather sharp vertical gradients encountered during the flights (see Fig. 1).

These ISOWAT measurements form an unprecedented dataset of tropospheric water vapour isotopologue profiles (high and well-documented level of accuracy and high vertical resolution). A more detailed report about the aircraft campaign, the ISOWAT measurements, and calibration procedures is currently prepared and will be subject of a separate paper.

2.2 Surface-based Picarro

Similar to ISOWAT the Picarro water isotopologue analyzers work with a tunable diode laser. The laser light enters a cavity filled with the airmass to be analysed. The

AMTD
7, 6917–6969, 2014

absorption signal of the airmass is determined by the ring-down time of the laser light intensity. In order to get an absorption spectrum the ring-down time is measured for different laser frequencies between 7183.5 and 7184 cm^{-1}. For more details please refer to the website of Picarro (http://www.picarro.com).

In March 2012 we installed a Picarro L2120-i water isotopologue analyzer at the Izaña Observatory at 2370 m a.s.l. The measured H_2O and δD time series is depicted in the left graphs of Fig. 2. Between October 2012 and March 2013 we had some instrumental problems and the instrument was sent to the manufacturer for repair. There are no measurements during this period. In June 2013 we installed an additional Picarro L2120-i analyzer at a small observatory located close to the cable car summit station of the Teide mountain (at 3550 m a.s.l.). The Teide H_2O and δD time series is depicted in the right graphs of Fig. 2. The time series document that the atmospheric water vapour fields are rather variable already on hourly time scales.

The δD calibration procedure for the Picarro instruments is based on a standard delivery module (SDM). It consists of two-syringe-pumps and allows injecting two different standards into the vaporizer where a constant dry air flow sustains immediate evaporation of the liquid in the air stream (for more details see also Aemisegger et al., 2012). The calibration is made every 8 h. It uses 2 different δD standards (at −142.2 ‰ and −245.3 ‰) that are analysed by the instrument at 3 different humidity levels covering the typical humidity range at Izaña and at Teide (during summer).

The precision of our 0.6 Hz measurements was 13.5 and 2 ‰ at 500 and 4500 ppmv, respectively. This noise almost completely averages out in the 10 min averages (our final data product). The random uncertainty of the individual calibrations (performed every 8 h) was 0.5 and 0.2 ‰ at 500 and 4500 ppmv, respectively, which also averages out on longer timescales. Systematic uncertainties of the used standard water and uncorrected humidity dependence were 1.7 and 0.7 ‰ at 500 and 4500 ppmv, respectively.

Our Picarro humidity data are calibrated with respect to humidity data measured by standard meteorological sensors. The humidity values measured by the Picarro and

AMTD
7, 6917–6969, 2014

the meteorological sensors are very strongly correlated and for the calibrated data we estimate a precision and accurcy of better than 2 %.

A more detailed description of the MUSICA Picarro in-situ measurements at Tenerife island is subject of a dedicated paper, which is currently in preparation (González et al., 2014).

3 The investigated remote sensing products

The characteristics of the water vapour isotopologue remote sensing products is rather complex. Schneider et al. (2012) introduce a proxy state concept that allows for reasonably characterising the interesting products, namely humidity (or H_2O) and δD (or HDO/H_2O). They identify two product types. Product type 1 is a vertically reasonably resolved H_2O profile and product type 2 is for isotopologue studies. Product type 2 provides H_2O and δD data that are representative for the same airmass and assures that the δD product is optimally independent on H_2O. In the following we use this proxy state concept for briefly discussing the characteristics of the MUSICA remote sensing products that are available for the area of Tenerife island.

3.1 Ground-based NDACC/FTIR

Ground-based FTIR remote sensing measurements have been performed at Izaña since 1999 (e.g., García et al., 2012). The experiment is situated in its own measurement laboratory (a shipping container equipped with electricity, air-conditioning, internet, etc.) and just about 50 m away from the Observatory's main building. Typically we measure on about 2–3 days per week. The number of measurement days is mainly limited by manpower, which is needed for operating the instrument. Ground-based FTIR systems measure high resolution mid-infrared solar absorption spectra. The spectra contain absorption signatures of many different atmospheric trace gases. Therefore, the technique can simultaneously monitor many different atmospheric trace

AMTD
7, 6917–6969, 2014

gases. Continuous developments of sophisticated retrieval algorithms allow also the retrieval of tropospheric water vapour isotopologues (for retrieval details please refer to Schneider et al., 2006b, 2010b).

The H_2O and δD apriori values applied for these isotoplogue retrievals are depicted in Fig. 1 as gray line. The MUSICA FTIR retrieval works with several spectral microwindows between 2655 and 3025 cm^{-1} and with HITRAN 2008 (Rothman et al., 2009) spectroscopic parameters, whereby the H_2O and HDO parameters have been adjusted for speed-dependent Voigt line shapes (Schneider et al., 2011), which affects pressure broading parameters but also line intensities. For H_2O the adjustment has been made taking coincident H_2O profile observations as the reference. For HDO the adjustment is more uncertain, since the atmospheric HDO state was calculated from the measured H_2O state assuming standard δD profiles (there were no HDO measurements available).

The left panel of graphs in Fig. 3 shows typical averaging kernels for the product type 1 {H_2O, δD}-state. The panel consists of 4 graphs. The upper left graph demonstrates how actual atmospheric H_2O affects retrieved H_2O, the upper right graph how actual atmospheric δD affects retrieved H_2O, the bottom right graph how actual atmospheric H_2O affects retrieved δD, and the bottom left graph how actual atmospheric δD affects retrieved δD. Product type 1 offers vertically reasonably resolved H_2O profile (FWHM, full width at half maximum, of kernels is 2 km in the lower troposphere, 4 km in the middle troposphere, and 6–8 km in the upper troposphere, Schneider et al., 2012), which have been empirically validated in a variety of previous studies (e.g., Schneider et al., 2006a, 2010a; Schneider and Hase, 2009). A further validation of product type 1 is not the subject of this paper.

Product type 2 is for isotopologue studies and shall be investigated in this paper. The type 2 product is calculated with the aposteriori correction method as presented in Schneider et al. (2012). The respective {H_2O, δD}-state averaging kernels are depicted as the graphs in the right panel of Fig. 3. The aposteriori correction significantly reduces the vertical resolution of the retrieved H_2O state (compare upper left graph

AMTD
7, 6917–6969, 2014

between the type 1 and type 2 panels). This sensitivity reduction is mandatory in order to assure that the H_2O product is representative for the same airmass as the δD product (compare upper left and bottom right graph in the type 2 panel). In addition, the aposteriori correction reduces the dependency of the retrieved δD on humidity, i.e., the cross dependency on humidity (compare the bottom left graphs between the type 1 and type 2 panels).

The Izaña FTIR product type 2 offers a degree of freedom for the signal (DOFS) for H_2O and δD of typically 1.75. The lower tropospheric kernels have an FWHM (Full Width at Half Maximum) of about 2 km and the middle tropospheric kernels an FWHM of about 5–6 km. In Schneider et al. (2012) the lower and middle tropospheric random uncertainty has been estimated to be smaller than 2 % for H_2O and 25 ‰ for δD, respectively, whereby measurement noise, spectral baseline uncertainties, and assumed tropospheric apriori temperature are the leading error sources. The systematic uncertainty can reach 10 % for H_2O and 150 ‰ for δD. It is dominated by uncertainties in the spectroscopic parameters (intensity and pressure broadening). The aposteriori correction method reduces the δD cross dependency on humidity to less than 10–15 ‰.

3.2 Space-based METOP/IASI

IASI is a Fourier transform spectrometer flown aboard the METOP satellites. It combines high temporal, horizontal, and spectral resolution (covers the whole globe twice per day, measures nadir pixels with a diameter of only 12 km, and records thermal radiation between 645 and 2760 cm^{-1} with a resolution of 0.5 cm^{-1}). IASI measurements are assured until 2020 on three different METOP satellites, whereby the first two are already in orbit: MetOp-A has been launched in October 2006, MetOp-B in September 2012. For our study we consider spectra measured by the IASI instruments aboard both satellites. Each IASI instrument has two Tenerife overpasses per day (about 10:30 and 22:30 UT). For MUSICA we work so far only with overpasses that observe clear sky scenes. We use very strict cloud screening conditions and therefore work with only about 10 % of all possible overpass spectra.

AMTD
7, 6917–6969, 2014

The retrieval uses the spectral window between 1190 and 1400 cm^{-1} and HITRAN 2008 (Rothman et al., 2009) spectroscopic line parameters. The applied apriori values are the same as for the FTIR retrievals and as depicted in Fig. 1 as gray line. Schneider and Hase (2011) present our IASI retrieval algorithm as well as a first theoretical error assessment of the respective H_2O and δD products.

The left panel of graphs in Fig. 4 shows typical averaging kernels for the product type 1 {H_2O, δD}-state of MUSICA IASI retrievals corresponding to spectra measured over the subtropical northern Atlantic. Product type 1 offers vertical H_2O profiles with the FWHM of the kernels of about 2 km in the lower and middle troposphere and 3 km in the upper troposphere (see upper left graph in type 1 panel of Fig. 4 and Schneider and Hase, 2011; Wiegele et al., 2014, for more a more detailed characterisation). The MUSICA product type 1 IASI H_2O profiles have are empirically validated in Schneider and Hase (2011) by comparison to meteorological radiosondes, ground-based FTIR, and EUMETSAT's METOP/IASI product and in Wiegele et al. (2014) by comparison to ground-based FTIR at three different locations (polar, mid-latitudinal, and subtropical) and a further validation of this type 1 product is not the subject of this paper.

Interesting for isotopologue studies is product type 2 which shall be further investigated in this paper. The respective {H_2O, δD}-state kernels are depicted in the right panel of graphs in Fig. 4. The sensitivity is typically limited to between 2 and 8 km altitude, with a maximum in the middle troposphere around 4–5 km. The random uncertainty for type 2 H_2O and δD is estimated to be about 5 % and 20 ‰, respectively, whereby measurement noise, surface emissivity, assumed tropospheric apriori temperature, and unrecognized thin elevated clouds are the leading error sources. The systematic uncertainty is very likely dominated by errors in the spectroscopic line parameters and can reach 2–5 % for H_2O in case of a 2–5 % error in the line intensity parameter. For δD the systematic uncertainty can reach 50 ‰ in case of inconsistencies of 5 % between the spectroscopic intensity parameters of H_2O and HDO. Despite the aposteriori correction there remains a δD cross dependency on humidity, which can cause an additional δD uncertainty of 30–50 ‰ (Wiegele et al., 2014).

AMTD
7, 6917–6969, 2014

4 Assessing random uncertainty and bias

Remote sensing data do not represent a single altitude. Instead they reflect the atmospheric situation as averaged out over a range of different altitudes (the kind of averaging is documented by the averaging kernels of Figs. 3 and 4). Such data can only be quantitatively compared to reference data that are available as vertical profiles. Here we compare the NDACC/FTIR and METOP/IASI products (product type 2, see Schneider et al., 2012) to the in-situ profiles as measured by ISOWAT between 200 and 6800 m a.s.l.

For a quantitative comparison we have to adjust the vertically highly-resolved ISOWAT profiles (x_{IW} as depicted in Fig. 1) to the modest vertical resolution of the remote sensing profiles. For this purpose we first perform an adjacent averaging towards the altitude grid of the remote sensing retrieval's forward model. The averaging is done for absolute number densities and ensures that the partial columns between two grid points is conserved. The adjacent averaging can be described by $\mathbf{M}x_{IW}$, whereby $\mathbf{M}$ is a $v \times w$ matrix with v and w being the numbers of the grid points of the forward model and of the vertically highly-resolved ISOWAT profile, respectively. In a second step we convolve $\mathbf{M}x_{IW}$ with the remote sensing averaging kernel $\hat{\mathbf{A}}$:

$$\hat{x}_{IW} = \hat{\mathbf{A}}(\mathbf{M}x_{IW} - x_a) + x_a \quad (2)$$

Here x_a is the apriori profile used by the remote sensing retrieval. When using the {H_2O, δD}-proxy state averaging kernels as depicted in Figs. 3 and 4 we have to make sure that $\mathbf{M}x_{IW}$ in Eq. (2) is in the {H_2O, δD}-proxy state. The result of this convolution is an ISOWAT profile ($\hat{x}_{IW}$) with the same vertical resolution as the remote sensing profile. In the following we will use the "hat"-index for marking parameters or amounts that result from convolution calculations according to Eq. (2).

The ISOWAT profiles are limited to 200–6800 m altitude, whereas the FTIR and IASI remote sensing instruments are also sensitive to altitudes above 7000 m (and IASI is also very weakly sensitive for altitudes below 200 m). For the comparison study we

AMTD
7, 6917–6969, 2014

extend the ISOWAT profiles above the aircrafts ceiling altitude by the values we use as apriori for the remote sensing retrievals (the apriori values are the same for FTIR and IASI and depicted as gray dashed line in Fig. 1). Below 200 m altitude we use the values as measured during the first 100 m of available aircraft data.

4.1 NDACC/FTIR

When comparing two atmospheric measurements we have to take care that the different instruments detect the same (or at least very similar) airmasses. Large differences in the vertical resolution can be accounted for by Eq. (2). In addition we have to be aware that ISOWAT measures the profile aboard a descending and ascending aircraft. Each flight, i.e., each ISOWAT profile measurement, takes about 3 h and is made over the ocean (see flight tracks of Fig. 5). This is in contrast to the FTIR remote sensing measurements, which need only about 10 min and are made at Izaña observatory at 2370 m a.s.l. on a mountain ridge of an island. It is well documented (e.g., Rodríguez et al., 2009) that the immediate surroundings of the island at this altitude are affected by mixing from the marine boundary layer (MBL). This mixing is mostly thermally driven: it is weak during the night and starts increasing during the morning hours and the airmass measured at or very close to the island becomes more and more affected by the MBL. At the end of the morning this airmass is not well representative for the situation encountered at the same altitude over the ocean.

For this study we compare the ISOWAT profile with the FTIR data obtained from the spectra measured in the morning with a solar elevation angle of 30°. This elevation assures that the FTIR has good sensitivity (absorption pathes are short enough and water vapour lines are not too heavily saturated) and it occurs only about 2:30 h after sunrise, when the influence of the MBL on the immediate surroundings of the island is still weak.

In Fig. 6 we compare the H_2O measurements. The data are depicted as difference to the apriori, i.e., we discuss here the variability that is actually introduced by the remote sensing measurement and observed by ISOWAT. Here and in the following we calculate

AMTD
7, 6917–6969, 2014

the H_2O differences as differences between the logarithms of the H_2O concentrations. Since $\Delta \ln X \approx \frac{\Delta X}{X}$ we can interpret these differences between the logarithms of the H_2O concentrations as relative differences. The graphs also show the predicted uncertainties for the lower and middle troposphere and for dry (day 130730) and humid conditions (day 130731). The respective error bars are hardly discernable, since the H_2O errors are only a few percent. Please note that the uncertainties as shown in the central graph take into account the assumption of climatologic apriori values for altitudes above the aircraft's ceiling altitude (no measurements!), which is the reason for the relative large uncertainty as estimated for the middle troposphere for the ISOWAT data smoothed by the FTIR kernels (central panel).

The comparison between the left and the central panels of Fig. 6 gives insight into the vertical structures that can be resolved by the remote sensing measurements. The profiles depicted in the central and the right panels represent the same vertical structures and their comparison allows conclusions about the quality of the remote sensing data.

For this purpose we statistically analyse the differences between the remote sensing product ($\hat{x}_{RS}$) and the convolved ISOWAT product ($\hat{x}_{IW}$, see Eq. 2). We determine the mean difference $\hat{b}_{DIFF}$ from the n numbers of coincidences:

$$\hat{b}_{DIFF} = \frac{1}{n} \sum_{i=1}^{n} (\hat{x}_{RS,i} - \hat{x}_{IW,i}) \quad (3)$$

and the standard deviation of the differences (the scatter between both data sets):

$$\hat{\sigma}_{DIFF} = \sqrt{\frac{1}{n} \sum_{i=1}^{n} (\hat{x}_{RS,i} - \hat{x}_{IW,i} - \hat{b}_{DIFF})^2} \quad (4)$$

Furthermore, we calculate the typical/mean scatter as predicted from the combined uncertainties of the remote sensing and the convolved ISOWAT data, $\hat{\epsilon}_{RS}$ and $\hat{\epsilon}_{IW}$,

AMTD
7, 6917–6969, 2014

respectively:

$$\hat{\epsilon}_{\mathrm{DIFF}} = \frac{1}{n}\sum_{i=1}^{n}\sqrt{\hat{\epsilon}^2_{\mathrm{RS},i} + \hat{\epsilon}^2_{\mathrm{IW},i}} \tag{5}$$

For comparison we also calculate a parameter, which is the scatter in the convolved ISOWAT data:

$$\hat{\sigma}_{\mathrm{IW}} = \sqrt{\frac{1}{n}\sum_{i=1}^{n}(\hat{x}_{\mathrm{IW},i} - \hat{\mu}_{\mathrm{IW}})^2} \tag{6}$$

whereby $\hat{\mu}_{\mathrm{IW}} = \frac{1}{n}\sum_{i=1}^{n}\hat{x}_{\mathrm{IW},i}$. The $\hat{\sigma}_{\mathrm{IW}}$ parameter informs about the random uncertainty of the water vapour state when no measurements are available (apriori uncertainty).

The values that result from these calculations for the comparison of FTIR and ISOWAT H_2O data are depicted in Fig. 7. In the left graph, the scatter between FTIR and ISOWAT (parameter $\hat{\sigma}_{\mathrm{DIFF}}$ according to Eq. 4) is shown as black triangles, together with the predicted scatter ($\hat{\epsilon}_{\mathrm{DIFF}}$ according to Eq. (5), red dashed line). We observe a scatter of about 28 % and 20 % for the lower and middle troposphere, respectively. In the lower troposphere the observed scatter is significantly larger than the scatter predicted from the combined uncertainties, which might be caused by the fact that the two instruments observe similar, but not the same airmasses. Especially for the lower troposphere where the FTIR airmass might be affected by local thermally driven small scale mixing processes. In this context the observed scatter can be interpreted as a rather conservative empirical estimation of the FTIR's random uncertainty. The blue solid line depicts the scatter between the six ISOWAT profiles when smoothed with the FTIR kernels (the $\hat{\sigma}_{\mathrm{IW}}$ values according to Eq. 6). It is much larger than the scatter in the difference with the FTIR profiles meaning that the FTIR well follows the ISOWAT reference, which confirms previous empirical validation exercises made for H_2O (e.g., Schneider et al., 2006a, 2010a; Schneider and Hase, 2009). Please note that the depicted red dashed line represents the combined uncertainty of the convolved ISOWAT

AMTD
7, 6917–6969, 2014

data and the FTIR data. The pure ISOWAT uncertainty (uncertainty of ISOWAT if not convolved with the FTIR kernel, ϵ_{IW}) is much smaller and depicted as blue dashed line.

The mean difference between FTIR and ISOWAT and the respective standard error of the mean ($\hat{b}_{DIFF}$ and $\hat{\sigma}_{DIFF}/\sqrt{n-1}$, according to Eqs. 3 and 4, respectively) are shown in the right graph of Fig. 7 as black triangles and error bars. The red area depicted around the zero line indicates the zone where a bias might be observed accidently due to the combined random uncertainties of ISOWAT and FTIR (this area is calculated as $\hat{\epsilon}_{DIFF}/\sqrt{n-1}$, see Eq. 5). The observed differences overlap well with this area meaning that there is no significant bias between the FTIR and the ISOWAT data.

The coincident δD profiles are shown in Fig. 8. Here the predicted uncertainties are clearly discernable. The results of the statistical analysis of the δD comparison are presented in Fig. 9. In the left graph we observe a scatter ($\hat{\sigma}_{DIFF}$) of about 45 ‰ and 15 ‰ for the lower and middle troposphere, respectively, which can be interpreted as a conservative empirical estimation of the FTIR's random uncertainty. In the middle troposphere this observed scatter is clearly smaller than the predicted one ($\hat{\epsilon}_{DIFF}$) indicating that our theoretical ISOWAT and/or FTIR error estimations might be too conservative. In particular the ISOWAT estimates are rather conservative since we assumed that on a single day all δD errors that occur at different altitudes and during ascend and decent are fully correlated. Allowing for δD errors that are not fully correlated (for instance positive errors at 2 km altitude and negative errors at 5 km altitude) would strongly decrease the error as estimated for the ISOWAT data, since through the convolution with the kernel a large part of the error would cancel out. The comparison of the observed scatter with the blue solid line (scatter between the six convolved ISOWAT profiles, $\hat{\sigma}_{IW}$) demonstrates that the FTIR δD product well captures the atmospheric variations as seen by the ISOWAT reference data.

The right graph of Fig. 9 reveals a clear systematic difference between the FTIR and the ISOWAT δD data. At and above 3 km altitude this difference lies outside the uncertainty area and is thus significant. It is about 25 ‰ in the lower troposphere and 70 ‰ in the middle troposphere.

AMTD
7, 6917–6969, 2014

In Fig. 10 we show a correlation plot for the H_2O and δD data as observed in the middle troposphere (altitude of 5 km) by ISOWAT and FTIR. This plot can serve as a summary of the comparison exercise: (1) H_2O and δD signals are similarly observed by both instruments (good correlation), (2) there is no significant difference between the H_2O data, and (3) there is a significant positive bias in the FTIR δD data.

4.2 METOP/IASI

The black circles in Fig. 5 show all the IASI pixels for morning overpasses that have been declared cloud free (according to EUMETSAT level 2 data) within a 250 km ×250 km area around the aircraft's flight tracks. In order to assure that IASI and ISOWAT observe similar airmasses we only work with IASI observations that are made not farer away than 50 km from the typical location of the aircraft. This yields 13 coincidences made on four different days: 130724, 130725, 130730, and 130731. The respective pixels are marked by red filled circles in Fig. 5.

IASI can hardly measure the vertical distribution of δD (see right panel of Fig. 4). For this reason we can limit the validation exercise to a single altitude level where IASI has typically good sensitivity. This is the case for the altitude of 5 km, which typically represents the atmospheric situation between 2 and 8 km altitude.

Figure 11 shows the same as Fig. 10 but for the IASI instead of the FTIR data. It depicts the correlation between the ISOWAT data (convolved with IASI kernels) and the IASI data. For H_2O the data group nicely around the 1 : 1 diagonal (except for three outliers on day 130731, which are marked by gray edges). For δD we also observe a nice correlation but there is a significant systematic difference. All the IASI data show rather consistently about 60 ‰ less HDO depletion than ISOWAT and this bias is outside the predicted uncertainty range, i.e., it is significant. In this context it is very interesting that for the FTIR data we observe almost the same systematic difference, which confirms the work of Schneider and Hase (2011) and Wiegele et al. (2014), where no systematic differences between IASI and FTIR are reported.

AMTD
7, 6917–6969, 2014

The good correlations as seen in Fig. 11 demonstrate that the IASI measurements significantly increases our knowledge of the atmospheric water vapour iotopologue state. In order to document this quantitatively, we compare the scatter observed in the difference between IASI and ISOWAT with the scatter observed in the ISOWAT profiles as well as with the scatter predicted from our ISOWAT and IASI uncertainty estimations. These scatter values are collected in Table 1. First, we see that the scatter in the IASI-ISOWAT difference (the value $\hat{\sigma}_{\mathrm{DIFF}}$ according to Eq. 4) is much smaller than the scatter in the convolved ISOWAT data (the value $\hat{\sigma}_{\mathrm{IW}}$ according to Eq. 6), i.e., IASI well tracks the H_2O and δD variations as observed by ISOWAT. From the $\hat{\sigma}_{\mathrm{DIFF}}$ values we empirically assess an IASI random uncertainty of better than 6–16 % for H_2O and about 13 ‰ for δD. For the latter the value is not larger than the combined estimated errors of the convolved ISOWAT and the IASI δD data ($\hat{\epsilon}_{\mathrm{DIFF}}$ according to Eq. 5), which is also about 13 ‰. Since ISOWAT and IASI actually do not detect the same airmass, part of the observed scatter should be due to the observation of a different airmass. Consequently our combined uncertainty estimations are very likely too conservative, which might be explained by the aforementioned conservative ISOWAT uncertainty assumption (assumption of fully correlated errors).

4.3 Bias in the remote sensing data

When comparing the remote sensing and ISOWAT H_2O data we find a systematic difference of up to 10 %. However, the mean difference is clearly smaller than the respective standard error of the mean, making this empirical bias estimation statistically insignificant (see black triangles and error bars in the right panel of Fig. 7). Since the lower/middle tropospheric H_2O fields are temporally and spatially very variable, it is difficult to identify a bias in the H_2O remote sensing product using a limited number of nearby in-situ reference observations.

In contrast to H_2O, the lower/middle tropospheric δD variability is small and a remote sensing δD bias might be detected even by using a small number of coinciding reference measurements. In fact the bias we observe between the few ISOWAT reference

AMTD
7, 6917–6969, 2014

data and our remote sensing δD product is statistically significant. It is between 1 % and 7 % for the FTIR (see right panels in Figs. 9 and 10) and about 6 % for the IASI data (see right panel of Fig. 11). However, these findings rely on very few comparisons made within a few days at a single location. In order to get a more reliable global estimate of the bias and for globally correcting the bias, further ISOWAT profile measurements at different sites and during different seasons would be desirable.

5 Proofing the added value of δD

5.1 The added value of δD observations

In Fig. 12 we plot all the in-situ data that have been measured so far in the lower or middle troposphere within the project MUSICA. These data represent different altitudes and two different locations (subtropics and mid-latitudes). We observe a strong correlation between the logarithm of H_2O concentrations and δD (linear correlation coefficient R^2 of about 80 %), which suggests that δD and H_2O contain similar information thereby relativising the results as presented in Sect. 4: in Fig. 9 and Table 1 we show that the remote sensing measurements can correctly detect a large part of the actual δD variations. However, we do not show if the remote sensing δD measurements are precise enough for detecting the small part of the lower/middle tropospheric δD variations that are complementary to H_2O.

In this context, we have to be aware that the remote sensing retrievals provide δD data that are slightly dependent on the atmospheric H_2O state (see the bottom left graphs in the type 1 and 2 panels of Figs. 3 and 4), meaning that the remote sensing δD data might be correlated to the in-situ δD data only via its dependency on H_2O and not because δD is correctly retrieved. The fact that in Sect. 4 we convolve the in-situ reference data with the remote sensing averaging kernels further increases this risk of misinterpreting the δD remote sensing data quality: by convolving the in-situ data with the averaging kernels we create a δD in-situ reference that has a similar dependency

AMTD
7, 6917–6969, 2014

on H_2O as the remote sensing data and the good correlation between the remote sensing and the convolved in-situ δD data might partly be a result of the convolution calculations according to Eq. (2).

For these reasons it is rather important to complement the quantitative validation exercises as shown in Sect. 4 by a qualitative study demonstrating that the δD remote sensing measurements add new information to the H_2O remote sensing data. This added value of δD can be examined by analysing δD-vs.-H_2O diagrams (we face a two dimensional validation problem!). In this section we work with pure in-situ data (not convolved with the remote sensing averaging kernels). This does not allow a quantitative study, but it ensures that our in-situ reference remains completely independent from the remote sensing data.

5.2 NDACC/FTIR vs. Picarro

For the analysis of δD-vs.-H_2O plots we need a large number of datapoints, that represent different atmospheric situations. Unfortunately, at the moment the number of ISOWAT profiles is very limited. As shown in Sect. 4 only six profiles coincide with ground-based FTIR observations and only four profiles with IASI measurements. Due to the small number of available ISOWAT reference data we cannot use the ISOWAT observations for validating the added value of the δD remote sensing measurements.

Instead we work with the in-situ reference data measured continuously by the Picarro L2120-i analyzers at Izaña and Teide. The airmasses detected by these instruments during nighttime/early morning are well representative for the free tropospheric conditions above Tenerife island (Rodríguez et al., 2009). The FTIR instrument is able to resolve the layer between Izaña and about 4 km above the island (see bottom right graph in the type 2 panel of Fig. 3). Hence, we should be able to qualitatively compare the early morning measurements of the Picarro and the FTIR instrument. IASI cannot resolve a layer above the island (see bottom right graph in the type 2 panel of Fig. 4) and thus we cannot compare Picarro and IASI observations.

AMTD
7, 6917–6969, 2014

A comparison of the Picarro and FTIR δD-vs.-H_2O curves is shown in Fig. 13, where we take the Izaña Picarro instrument as the reference. We find 85 days where early morning Picarro and FTIR measurements coincide. The upper graphs show the respective Picarro measurements. We are interested in the δD signal that is anomalous with respect to the typically observed correlation between δD and ln[H_2O]. Therefore, we determine a second order regression line between δD and ln[H_2O] and classify two types of δD anomalies. The first type is existent when all the Picarro δD values measured during the morning of the same day lie above the regression line. There are 30 days with this anomaly and they can be identified in the upper left panel of Fig. 13 by the olive crosses. The second type of δD anomalies is existent when all the δD values of a single day lie below the regression line. These anomalies occur on other 30 days and are marked by the green crosses in the right panel.

Then we investigate if the δD anomalies as seen by the Picarro are observed in the coincident FTIR measurements. For this purpose we plot the FTIR δD-vs.-H_2O and mark the data according to the anomalies as identified by the Picarro observations. These plots are presented in the bottom panels of Fig. 13. On days where the Picarro observes unusually high δD values the coincident FTIR measurements reveal a very similar anomaly (see olive crosses in the left panels). And vice versa, the observation of unusually low δD values as made by the Picarro is also seen in the coincident FTIR data (see green crosses in the right panels).

Figure 14 shows the same kind of comparison, but taking the Picarro instrument installed at Teide mountain as reference. There the number of coincidences is smaller (Teide Picarro measurements started more than one year after the respective Izaña measurements), but we also see a reasonable agreement for the anomalies as detected by Picarro and FTIR.

5.3 Dehydration via condensation vs. vertical mixing from the boundary layer

The downwelling branch of the Hadley circulation plays a dominating role for the free troposphere (FT) of the subtropics. It is responsible for a strong subsidence inversion

AMTD
7, 6917–6969, 2014

layer which hinders mixing of planetary boundary layer (PBL) air into the FT. Under such situation the FT airmass is transported from higher latitudes and/or higher altitudes (Galewsky et al., 2005; Barnes and Hartmann, 2010; Cuevas et al., 2013).

In addition the summertime FT of the northern subtropical Atlantic is frequently affected by airmasses that are advected from the African continent (e.g., Prospero et al., 2002; Rodríguez et al., 2011; Andrey et al., 2014). At that time of the year there are strong and extended heat lows over the African continent at 20–35° N. These heat lows modify the transport pathways to the FT and enable mixing from the PBL to the FT (e.g., Valero et al., 1992).

These two different transport pathways can be observed at our reference site (island of Tenerife and surroundings) during the summer season, and we can use these circumstances for validating the added value of the δD signal.

5.3.1 Aerosol data as proxy for transport pathways

Saharan dust aerosols measured in the FT around Tenerife can be used for identifying an airmass that has experienced vertical transport over the African continent. This shall be demonstrated by Fig. 15, which shows that at Izaña and in summer high aerosol concentrations ($PM_{10} > 25\,\mu g\,m^{-3}$) are clearly correlated to airmasses that have been advected from the African continent. The PM_{10} aerosol data is the aerosol mass concentration considering all particles with aerodynamic diameter smaller than 10 µm, and at Izaña, PM_{10} is, by far, dominated by Saharan dust particles (Rodríguez et al., 2011). For the calculation of the backward trajectories we use HYSPLIT (Hybrid Single-Particle Lagrangian Integrated Trajectory, some examples and explanations of the HYSPLIT calculations are given in Cuevas et al., 2013).

In the following we use low aerosol concentrations as proxy for a FT airmass that has been mainly transported from higher latitudes and/or higher altitudes (clean conditions, no vertical mixing from the PBL to the FT). High aerosol concentrations are our proxy for airmasses influenced by vertical mixing over the African continent (dust conditions). We investigate the isotopologue data measured by the different instruments under the

AMTD
7, 6917–6969, 2014

different conditions. For each instrument we need aerosol data that are representative for a similar airmass as the isotopologue data.

For ISOWAT we use the V_{10} aerosol data observed in-situ during the flights. The V_{10} aerosol data is the aerosol volume concentration considering particles with a diameter smaller than 10 µm. The vertical resolution of these measurements is 100 m. The ISOWAT data are much higher resolved. We calculate 100 m averages from the ISOWAT data in order to make them representative for the same layers as the aerosol data. An airmass with $V_{10} < 1\,\mu m^3\,cm^{-3}$ is defined as a clean airmass and an airmass with $V_{10} > 10\,\mu m^3\,cm^{-3}$ is defined as dust airmass. For more details on the aircraft aerosol data please refer to the appendix and Fig. A1.

The Izaña Picarro data are paired with Izaña's PM_{10} in-situ aerosol measurements. As definition for clean conditions we use $PM_{10} < 2\,\mu g\,m^{-3}$ and for dust conditions $PM_{10} > 25\,\mu g\,m^{-3}$. More information about this data is given in the appendix (Fig. A2). We only work with nighttime data. Thereby we can well exclude data that are affected by local mixing between the MBL and the FT.

At Teide there are no continuous in-situ aerosol observations and we pair the Teide Picarro data with the Izaña AERONET (http://aeronet.gsfc.nasa.gov) remote sensing data. The AERONET photometers analyse the direct sunlight and report the aerosol optical depth (AOD) for the whole atmosphere above Izaña, i.e., they are reasonably representative for the altitudes around Teide. For an AOD value at 500 nm below 2.5×10^{-2} we assume clean conditions and above 5×10^{-2} dust conditions. In order to avoid influences from local vertical mixing we only work with morning data. Please note that we cannot work with nighttime data, since the AERONET photometers need direct sunlight.

Izaña's ground-based FTIR remote sensing system has the capability to resolve the first few kilometers above Izaña. The Izaña AERONET data are representative for similar airmasses and can be used for classifying the FTIR data. We use the same threshold levels as for the the classification of the Teide Picarro data. We only work with measurements made in morning hours (solar elevation of below 30°).

AMTD
7, 6917–6969, 2014

For the classification of the IASI data we also use Izaña's AERONET data. However, we have to consider that IASI is most sensitive at around 5 km altitude, i.e., an altitude significantly above the location of the Izaña AERONET photometer. In order to have a reasonable proxy for aerosol amounts around 5 km altitude we work with higher AOD threshold values. We use a value below 3×10^{-2} for clean conditions and above 1.5×10^{-1} for dust conditions.

5.3.2 Identifying the transport pathways in the water vapour isotopologue data

Figure 16 shows the δD-vs.-H_2O plots for the different instruments (from the top to the bottom: ISOWAT, Picarro at Izaña, Picarro at Teide, ground-based FTIR, and IASI). We only work with data measured during summer (May–October). Gray dots represent all measurements. The blue dots (left panels) represent the observations made for clean conditions, i.e., when there is weak/no influence from the African continent. The red dots (right panels) are for observations made for dust conditions, i.e., when the airmass is clearly affected by vertical mixing over Africa.

The top graphs show the ISOWAT data together with simulated δD-vs.-H_2O curves. The magenta line represents values that occur for mixing of two airmasses: a humid airmass with MBL values (H_2O: 25000 ppmv; δD: −80 ‰) and a dry FT background airmass (H_2O: 900 ppmv; δD: −430 ‰). The cyan line represents a Rayleigh distillation curve for an initial atmospheric temperature of 25 °C, a relative humidity at the surface of 80 %, and an averaged thermodynamic profile. Rayleigh distillation means that all water that condenses during the transport pathway is immediately removed from the airmass. There is a strong correlation between the ISOWAT water vapour isotopologue data and the aerosol proxy: (1) when vertical mixing over Africa is clearly discernable in the aerosol data, the ISOWAT δD data group around a mixing line. (2) When the aerosol data reveal no significant vertical mixing over Africa the δD data approximate towards a Rayleigh distillation line (blue dots and cyan line in the top graphs of Fig. 16).

These different transport pathways are also well observed in the in-situ isotopologue datasets as collected by the two Picarros at Izaña and Teide. In particular the Picarro

AMTD
7, 6917–6969, 2014

at Izaña provides a very large data set (it has been continuously operating in summer 2012 and 2013), hence these findings are very robust.

The two lowermost rows of graphs show the respective plots for the FTIR and IASI datasets, which are representative for several years. We work with FTIR data measured during summertime morning hours between 2005 and 2013, where we have a good overlap with the AERONET data. We use IASI-A data measured between October 2007 and the end of July 2013 as well as with a few 2013 IASI-B data (from June/July 2013). All remote sensing datasets reveal the different transport pathways similarly to the in-situ datasets. This qualitative similarity well demonstrates that the MUSICA FTIR and IASI δD remote sensing data add scientifically useful information to the respective H_2O measurement.

A more profound scientific examination of these different transport regimes is out of the scope of this technical validation paper and shall be addressed in an extra paper which is currently in preparation (González et al., 2014).

6 Conclusions

Global remote sensing of tropospheric δD in addition to H_2O can open up novel opportunities for tropospheric water cycle research. However, the interesting signal of the added value of δD is small. Its detection by remote sensing techniques is a difficult task and prior to a scientific application of the data, their characteristics and uncertainties should be well understood. In this context Schneider et al. (2012) and Wiegele et al. (2014) show detailed feasibility and error assessment studies for MUSICA's NDACC/FTIR and METOP/IASI water vapour isotopologue products. In this paper those efforts are complemented by an empirical validation exercise taking high quality in-situ measurements as the reference.

For a quantitative validation of the random uncertainty and the bias of the remote sensing data we need in-situ observations of well-resolved vertical profiles. During an aircraft campaign in July 2013 we produce six of such profiles using the dedicated

AMTD
7, 6917–6969, 2014

aircraft instrument ISOWAT, whose extensive pre-, post-, and in-flight calibration modes ensure data of high accuracy and a very high vertical resolution. With this unprecedented dataset and based on the scatter between the coincident ISOWAT and remote sensing observations we can assess the random uncertainty of the NDACC/FTIR δD product to be smaller than 45 ‰ and 15 ‰ for the lower and middle troposphere, respectively. For the middle tropospheric METOP/IASI δD product we assess a value of 13 ‰. For the bias assessment we examine systematic differences with respect to ISOWAT and find that there is a systematic positive difference of about 30–70 ‰, which is similarly observed for the NDACC/FTIR and the METOP/IASI δD product. For a global and more reliable bias estimation we need more reference profiles measured at a variety of globally representative sites (currently we only have six coinciding reference profiles for one single location).

The quantitative comparison to the ISOWAT data does not demonstrate whether the remote sensing δD data is complementary to the remote sensing H_2O data. Such complementarity has to be investigated by δD-vs.-H_2O plots. For these plots we need a large number of datapoints, thus they are not possible by means of only six ISOWAT profiles. Instead we use the Izaña and Teide Picarro instruments, whose early morning observations can serve as qualitative reference for the ground-based FTIR data. We are able to demonstrate that the FTIR δD data adds a similar value to the FTIR H_2O data than the Picarro δD data to the Picarro H_2O data. Furthermore, we are able to demonstrate that all the instruments involved in our study (ISOWAT, Picarro at Izaña and Teide, NDACC/FTIR, and METOP/IASI) are able to consistently identify two different free tropospheric water vapour transport pathways. Transport from the PBL via vertical mixing can be identified by isotopologue data that approximate a mixing line on the δD-H_2O surface. Such mixing lines occur in all datasets primarily in the presence of large aerosol amounts, which serve as proxy for large scale vertical mixing over the African continent. On the contrary and if there are small aerosol amounts we observe primarily δD-vs.-H_2O curves that approximate a Rayleigh curve, meaning that the respective airmasses have been dried by condensation. This is in agreement

AMTD
7, 6917–6969, 2014

with a strong inversion layer that hinders mixing from the PBL and prevailing moisture transport from higher latitudes.

Our study proves that the MUSICA H_2O and δD remote sensing data are a reliable tool for water vapor isotopologue studies. However, we have to be aware that there is very likely a bias in the δD values. For a better understanding of this bias further research on the spectroscopic line parameters as well as more high quality aircraft profiles and thus further campaigns and validation efforts would be desirable.

We would like to propose using the approaches as presented in this paper, in Schneider et al. (2012), and in Wiegele et al. (2014) as guideline for best practices when validating water vapour isotopologue remote sensing datasets.

Appendix A: The aerosol datasets

The INTA aerosol instrument provides the aerosol number density for different particle sizes, whereby different particle sizes ranging from 0.5 to 50 µm diameter can be distinguished. From these data we calculate the aerosol volume concentration for all the aerosols with a diameter smaller than 10 µm (this volume concentration is called V_{10}), whereby we assume spherical aerosols. The respective data measured during the six flights above the boundary layer (above 1500 m a.s.l.) are plotted in Fig. A1. Please note that there are many occasions with $V_{10} = 0\,\mu m^3\,cm^{-3}$ (aerosol number density below the detection limit) that are not visible in the graph.

The Izaña PM_{10} data are hourly averaged mass concentration data and given as aerosol mass per air volume. Figure A2 shows the 2012–2013 time series. The mass concentrations are determined from the continuously measured aerosol size distributions (applying the instrument APS, TSI^{TM}, model 3321). First the aerosol volume concentrations (V_{10}) are calculated. From V_{10} the mass concentration (PM_{10}) is obtained by using an empirically estimated aerosol effective density using the methods described by (Rodríguez et al., 2012). This density estimation consists in correlating the measured aerosol volume concentrations to mass concentrations measured by the

AMTD
7, 6917–6969, 2014

gravimetric method. For the gravimetric method PM_{10} aerosols are collected in microfiber quartz filters. This collection needs several hours and requires a careful treatment of the filters, hence the gravimetric method cannot be performed continuously. The Izaña programme for in-situ aerosol characterization was audited by the World Calibration Centre for Aerosol Physics (WCCAP; Institute for Tropospheric Research, Leipzig) in November 2006. For more details on these PM_{10} data please refer to Rodríguez et al. (2011).

The Aerosol Robotic Network (AERONET) provides atmospheric aerosol properties at several wavelengths (Holben et al., 1998). The Cimel CE-318 sun photometer is the standard instrument in the network. It measures direct sun irradiance (every 15 min) with a 1.2° full field of view that is used to compute aerosol optical depth (AOD) for each wavelength available on each photometer type. Three quality levels of AERONET data are available: level 1.0 (real time raw data), level 1.5 (real time cloud screened data), and level 2.0 (quality assured data). Figure A3 shows the time series of AOD at 500 nm as measured at the Izaña observatory.

Acknowledgements. This study has been conducted in the framework of the project MUSICA which is funded by the European Research Council under the European Community's Seventh Framework Programme (FP7/2007–2013)/ERC Grant agreement number 256961.

E. Sepúlveda is supported by the Ministerio de Economía and Competitividad of Spain for the project NOVIA (CGL2012-37505).

The aircraft campaign has been co-funded by the project MUSICA and the Spanish national project AMISOC (CGL2011-24891).

We are grateful to INTA Aerial Platforms, a branch of the Spanish ICTS program, and the Spanish Air Force for their efforts in maintaining and operating the aircraft.

The Izaña aerosol in-situ measurements are part of the project POLLINDUST (CGL2011-26259) funded by the Minister of Economy and Competitiveness of Spain.

The AERONET sun photometer at Izaña (PI: Emilio Cuevas) has been calibrated within AERONET EUROPE TNA supported by the European Community Research Infrastructure Action under the FP7 Capacities program for Integrating Activities, ACTRIS grant agreement number 262254.

AMTD
7, 6917–6969, 2014

We acknowledge the support by the Deutsche Forschungsgemeinschaft and the Open Access Publishing Fund of the Karlsruhe Institute of Technology.

The service charges for this open access publication have been covered by a Research Centre of the Helmholtz Association.

References

Aemisegger, F., Sturm, P., Graf, P., Sodemann, H., Pfahl, S., Knohl, A., and Wernli, H.: Measuring variations of $\delta^{18}O$ and $\delta^{2}H$ in atmospheric water vapour using two commercial laser-based spectrometers: an instrument characterisation study, Atmos. Meas. Tech., 5, 1491–1511, doi:10.5194/amt-5-1491-2012, 2012. 6923

Andrey, J., Cuevas, E., Parrondo, M. C., Alonso-Pérez, S., Redondas, A., and Gil-Ojeda, M.: Quantification of ozone reductions within the Saharan air layer through a 13-year climatologic analysis of ozone profiles, Atmos. Environ., 84, 28–34, doi:10.1016/j.atmosenv.2013.11.030, 2014. 6938

Barnes, E. A. and Hartmann, D. L.: Influence of eddy-driven jet latitude on North Atlantic jet persistence and blocking frequency in CMIP3 integrations, Geophys. Res. Lett., 37, L23802, doi:10.1029/2010GL045700, 2010. 6938

Boesch, H., Deutscher, N. M., Warneke, T., Byckling, K., Cogan, A. J., Griffith, D. W. T., Notholt, J., Parker, R. J., and Wang, Z.: HDO/H_2O ratio retrievals from GOSAT, Atmos. Meas. Tech., 6, 599–612, doi:10.5194/amt-6-599-2013, 2013. 6919, 6920

Craig, H.: Standard for reporting concentrations of deuterium and oxygen-18 in natural waters, Science, 13, 1833–1834, doi:10.1126/science.133.3467.1833, 1961. 6919

Cuevas, E., González, Y., Rodríguez, S., Guerra, J. C., Gómez-Peláez, A. J., Alonso-Pérez, S., Bustos, J., and Milford, C.: Assessment of atmospheric processes driving ozone variations

AMTD
7, 6917–6969, 2014

in the subtropical North Atlantic free troposphere, Atmos. Chem. Phys., 13, 1973–1998, doi:10.5194/acp-13-1973-2013, 2013. 6938
Dyroff, C., Fütterer, D., and Zahn, A.: Compact diode-laser spectrometer ISOWAT for highly sensitive airborne measurements of water-isotope ratios, Appl. Phys. B, 98, 537–548, doi:10.1007/s00340-009-3775-6, 2010. 6921
Frankenberg, C., Yoshimura, K., Warneke, T., Aben, I., Butz, A., Deutscher, N., Griffith, D., Hase, F., Notholt, J., Schneider, M., Schrejver, H., and Röckmann, T.: Dynamic processes governing lower-tropospheric HDO/H_2O ratios as observed from space and ground, Science, 325, 1374–1377, doi:10.1126/science.1173791, 2009. 6919
Frankenberg, C., Wunch, D., Toon, G., Risi, C., Scheepmaker, R., Lee, J.-E., Wennberg, P., and Worden, J.: Water vapor isotopologue retrievals from high-resolution GOSAT shortwave infrared spectra, Atmos. Meas. Tech., 6, 263–274, doi:10.5194/amt-6-263-2013, 2013. 6919
Galewsky, J., Sobel, A., and Held, I.: Diagnosis of subtropical humidity dynamics using tracers of last saturation journal of the atmospheric sciences, Atmos. Sci., 62, 3353–3367, doi:10.1175/jas3533.1, 2005. 6938
García, O. E., Schneider, M., Redondas, A., González, Y., Hase, F., Blumenstock, T., and Sepúlveda, E.: Investigating the long-term evolution of subtropical ozone profiles applying ground-based FTIR spectrometry, Atmos. Meas. Tech., 5, 2917–2931, doi:10.5194/amt-5-2917-2012, 2012. 6924
González, Y., Schneider, M., Rodríguez, S., Dyroff, C., Christner, E., García, O. E., and Sepúlveda, E.: Water vapour isotopologue fingerprints of the Saharan Air Layer and North Atlantic free troposphere in the Subtropical North Atlantic region, Atmos. Chem. Phys. Discuss., in preparation. 2014. 6924, 6941
Holben, B. N., Eck, T. F., Slutsker, I., Tanre, D., Buis, J., Setzer, A., Vermote, E., Reagan, J., Kaufman, Y., Nakajima, T., Lavenu, F., Jankowiak, I., and Smirnov, A.: AERONET – a federated instrument network and data archive for aerosol characterization, Remote Sens. Environ., 66, 1–16, 1998. 6944
Lacour, J.-L., Risi, C., Clarisse, L., Bony, S., Hurtmans, D., Clerbaux, C., and Coheur, P.-F.: Mid-tropospheric δD observations from IASI/MetOp at high spatial and temporal resolution, Atmos. Chem. Phys., 12, 10817–10832, doi:10.5194/acp-12-10817-2012, 2012. 6919, 6920
Prospero, J. M., Ginoux, P., Torres, O., Nicholson, S. E., and Gill, T. E.: Environmental characterizacion of global sources of dust with the Nimbus 7 Total Ozone Map-

AMTD
7, 6917–6969, 2014

ping Spectrometer (TOMS) absorbing aerosol product, Rev. Geophys., 40, 2–1–2–31, doi:10.1029/2000RG000095, 2002. 6938

Risi, C., Noone, D., Worden, J., Frankenberg, C., Stiller, G., Kiefer, M., Funke, B., Walker, K., Bernath, P., Schneider, M., Bony, S., Lee, J., Brown, D., and Sturm, C.: Process-evaluation of tropospheric humidity simulated by general circulation models using water vapor isotopic observations. Part 2: An isotopic diagnostic to understand the mid and upper tropospheric moist bias in the tropics and subtropics, J. Geophys. Res., 117, D05304, doi:10.1029/2011JD016623, 2012. 6919

Rodríguez, S., González, Y., Cuevas, E., Ramos, R., Romero, P. M., Abreu-Afonso, J., and Redondas, A.: Atmospheric nanoparticle observations in the low free troposphere during upward orographic flows at Izaña Mountain Observatory, Atmos. Chem. Phys., 9, 6319–6335, doi:10.5194/acp-9-6319-2009, 2009. 6929, 6936

Rodríguez, S., Alastuey, A., Alonso-Pérez, S., Querol, X., Cuevas, E., Abreu-Afonso, J., Viana, M., Pérez, N., Pandolfi, M., and de la Rosa, J.: Transport of desert dust mixed with North African industrial pollutants in the subtropical Saharan Air Layer, Atmos. Chem. Phys., 11, 6663–6685, doi:10.5194/acp-11-6663-2011, 2011. 6938, 6944

Rodríguez, S., Alastuey, A., and Querol, X.: A review of methods for long term in situ characterization of aerosol dust, Aeolian Research, 6, 55–74, doi:10.1016/j.aeolia.2012.07.004, 2012. 6943

Rothman, L. S., Gordon, I. E., Barbe, A., Chris Benner, D., Bernath, P. F., Birk, M., Boudon, V., Brown, L. R., Campargue, A., Champion, J.-P., Chance, K., Coudert, L. H., Dana, V., Devi, V. M., Fally, S., Flaud, J.-M., Gamache, R. R., Goldman, A., Jacquemart, D., Kleiner, I., Lacome, N., Lafferty, W. J., Mandin, J.-Y., Massie, S. T., Mikhailenko, S. N., Miller, C. E., Moazzen-Ahmadi, N., Naumenko, O. V., Nikitin, A. V., Orphal, J., Perevalov, V. I., Perrin, A., Predoi-Cross, A., Rinsland, C. P., Rotger, M., Simecková, M., Smith, M. A. H., Sung, K., Tashkun, S. A., Tennyson, J., Toth, R. A., Vandaele, A. C., and Vander-Auwera, J.: The HITRAN 2008 molecular spectroscopic database, J. Quant. Spectrosc. Radiat. Transfer, 110, 533–572, doi:10.1016/j.jqsrt.2009.02.013, 2009. 6925, 6927

Schmidt, G. A., Hoffmann, G., Shindell, D. T., and Hu, Y.: Modeling atmospheric stable water isotopes and the potential for constraining cloud processes and stratosphere-troposphere water exchange, J. Geophys. Res., 110, D21314, doi:10.1029/2005JD005790, 2005. 6919

Schneider, M. and Hase, F.: Ground-based FTIR water vapour profile analyses, Atmos. Meas. Tech., 2, 609–619, doi:10.5194/amt-2-609-2009, 2009. 6925, 6931

AMTD
7, 6917–6969, 2014

Schneider, M. and Hase, F.: Optimal estimation of tropospheric H_2O and δD with IASI/METOP, Atmos. Chem. Phys., 11, 11207–11220, doi:10.5194/acp-11-11207-2011, 2011. 6919, 6920, 6927, 6933

Schneider, M., Hase, F., and Blumenstock, T.: Water vapour profiles by ground-based FTIR spectroscopy: study for an optimised retrieval and its validation, Atmos. Chem. Phys., 6, 811–830, doi:10.5194/acp-6-811-2006, 2006a. 6925, 6931

Schneider, M., Hase, F., and Blumenstock, T.: Ground-based remote sensing of HDO/H_2O ratio profiles: introduction and validation of an innovative retrieval approach, Atmos. Chem. Phys., 6, 4705–4722, doi:10.5194/acp-6-4705-2006, 2006b. 6919, 6925

Schneider, M., Romero, P. M., Hase, F., Blumenstock, T., Cuevas, E., and Ramos, R.: Continuous quality assessment of atmospheric water vapour measurement techniques: FTIR, Cimel, MFRSR, GPS, and Vaisala RS92, Atmos. Meas. Tech., 3, 323–338, doi:10.5194/amt-3-323-2010, 2010a. 6925, 6931

Schneider, M., Toon, G. C., Blavier, J.-F., Hase, F., and Leblanc, T.: H_2O and δD profiles remotely-sensed from ground in different spectral infrared regions, Atmos. Meas. Tech., 3, 1599–1613, doi:10.5194/amt-3-1599-2010, 2010b. 6925

Schneider, M., Hase, F., Blavier, J.-F., Toon, G. C., and Leblanc, T.: An empirical study on the importance of a speed-dependent Voigt line shape model for tropospheric water vapor profile remote sensing, J. Quant. Spectrosc. Ra., 112, 465–474, doi:10.1016/j.jqsrt.2010.09.008, 2011. 6925

Schneider, M., Barthlott, S., Hase, F., González, Y., Yoshimura, K., García, O. E., Sepúlveda, E., Gomez-Pelaez, A., Gisi, M., Kohlhepp, R., Dohe, S., Blumenstock, T., Wiegele, A., Christner, E., Strong, K., Weaver, D., Palm, M., Deutscher, N. M., Warneke, T., Notholt, J., Lejeune, B., Demoulin, P., Jones, N., Griffith, D. W. T., Smale, D., and Robinson, J.: Ground-based remote sensing of tropospheric water vapour isotopologues within the project MUSICA, Atmos. Meas. Tech., 5, 3007–3027, doi:10.5194/amt-5-3007-2012, 2012. 6919, 6924, 6925, 6926, 6928, 6941, 6943, 6953, 6954

Valero, F., Luna, Y., Martín, M., and Sancho, P.: Tropospheric ozone concentrations related to atmospheric conditions at Izaña BAPMoN weather station, Canary Islands, Il Nuovo Cimento C, 15, 159–172, doi:10.1007/BF02507610, 1992. 6938

Webster, C. R. and Heymsfield, A. J.: Water isotope ratios H/D, $^{18}O/^{16}O$, $^{17}O/^{16}O$ in and out of clouds map dehydration pathways, Science, 302, 1742–1745, doi:10.1126/science.1089496, 2003. 6919

AMTD
7, 6917–6969, 2014

Wiegele, A., Schneider, M., Hase, F., Barthlott, S., García, O. E., Sepúlveda, E., González, Y., Blumenstock, T., Raffalski, U., Gisi, M., and Kohlhepp, R.: The MUSICA MetOp/IASI H_2O and δD products: characterisation and long-term comparison to NDACC/FTIR data, Atmos. Meas. Tech. Discuss., 7, 3915–3952, doi:10.5194/amtd-7-3915-2014, 2014. 6927, 6933, 6941, 6943, 6954

Worden, J. R., Bowman, K., Noone, D., Beer, R., Clough, S., Eldering, A., Fisher, B., Goldman, A., Gunson, M., Herman, R., Kulawik, S. S., Lampel, M., Luo, M., Osterman, G., Rinsland, C., Rodgers, C., Sander, S., Shephard, M., and Worden, H.: TES observations of the tropospheric HDO/H_2O ratio: retrieval approach and characterization, J. Geophys. Res., 11, D16309, doi:10.1029/2005JD006606, 2006. 6919

Worden, J., Noone, D., Bowman, K., Beer, R., Eldering, A., Fisher, B., Gunson, M., Goldman, A., Herman, R., Kulawik, S. S., Lampel, M., Osterman, G., Rinsland, C., Rodgers, C., Sander, S., Shephard, M., Webster, R., and Worden, H.: Importance of rain evaporation and continental convection in the tropical water cycle, Nature, 445, 528–532, doi:10.1038/nature05508, 2007. 6919

Worden, J., Noone, D., Galewsky, J., Bailey, A., Bowman, K., Brown, D., Hurley, J., Kulawik, S., Lee, J., and Strong, M.: Estimate of bias in Aura TES HDO/H_2O profiles from comparison of TES and in situ HDO/H_2O measurements at the Mauna Loa observatory, Atmos. Chem. Phys., 11, 4491–4503, doi:10.5194/acp-11-4491-2011, 2011. 6920

AMTD
7, 6917–6969, 2014

Table 1. Scatter values as obtained from IASI and ISOWAT coincidences that fulfill our coincidence criteria (presents the same as the left panels of Figs. 7 and 9, but for IASI instead of FTIR and at 5 km altitude only). Predicted: combined ISOWAT and IASI estimated uncertainties ($\hat{\epsilon}_{\mathrm{DIFF}}$); IASI-ISOWAT: scatter as observed in the difference between ISOWAT and IASI ($\hat{\sigma}_{\mathrm{DIFF}}$); ISOWAT: scatter as observed in the ISOWAT data ($\hat{\sigma}_{\mathrm{IW}}$). The values in parenthesis are for calculations without considering the three outliers on 130731.

	H_2O [%]	δD [‰]
Predicted ($\hat{\epsilon}_{\mathrm{DIFF}}$)	9.9 (8.5)	13.2 (12.3)
IASI-ISOWAT ($\hat{\sigma}_{\mathrm{DIFF}}$)	16.0 (6.0)	12.0 (13.2)
ISOWAT ($\hat{\sigma}_{\mathrm{IW}}$)	29.9 (34.4)	37.1 (36.7)

AMTD
7, 6917–6969, 2014

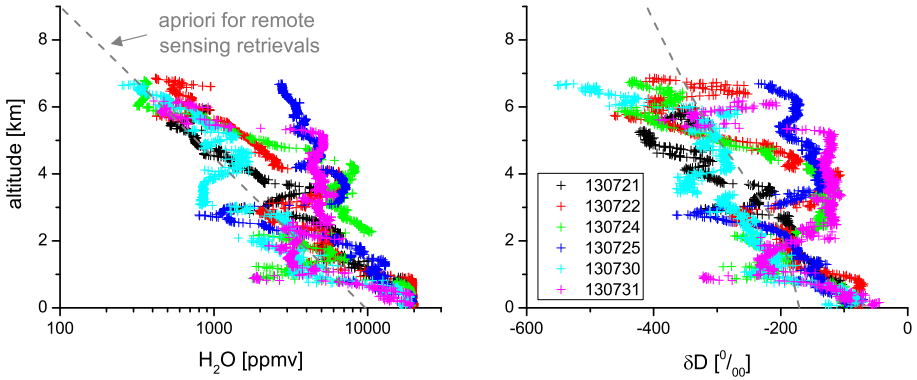

Figure 1. H_2O (left graph) and δD profiles (right graph) as measured by ISOWAT above the subtropical Atlantic close to Tenerife between 10:00 and 13:00 UT during six days on the end of July 2013. The depicted data are 10 m vertical averages. For comparison we also depict the apriori profiles used for the MUSICA NDACC/FTIR and METOP/IASI remote sensing retrievals (gray dashed lines).

AMTD
7, 6917–6969, 2014

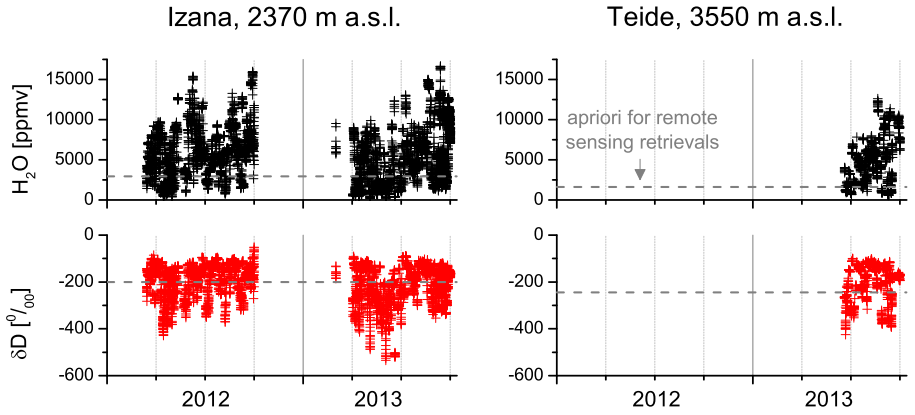

Figure 2. H_2O (upper graph) and δD data (bottom graph) as measured by the Picarro instruments on Tenerife between 06:00 and 08:00 UT. The depicted data are 10 min averages. For comparison we also depict the apriori values used for the MUSICA NDACC/FTIR and METOP/IASI remote sensing retrievals (gray dashed lines).

AMTD
7, 6917–6969, 2014

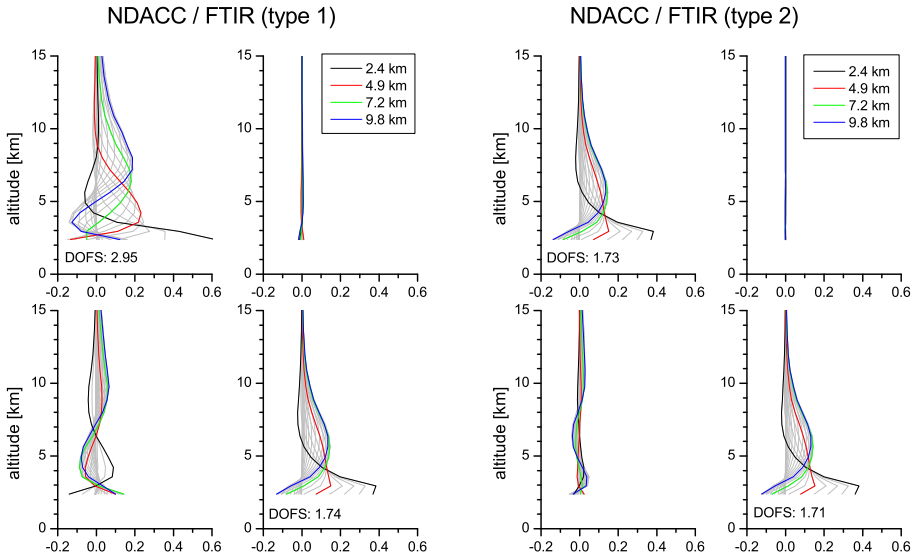

Figure 3. Typical row kernels for the {H_2O, δD}-proxy states as retrieved from Izaña's ground-based NDACC/FTIR spectra. Left panel of graphs: product type 1 kernels; right panel of graphs: product type 2 kernels. The upper graphs of each panel display how the retrieved H_2O is affected by actual H_2O variations (left graph) and by actual δD variations (right graph). The lower graphs of each panel display the same for the retrieved δD. For more details on the proxy state kernels please refer to (Schneider et al., 2012).

AMTD
7, 6917–6969, 2014

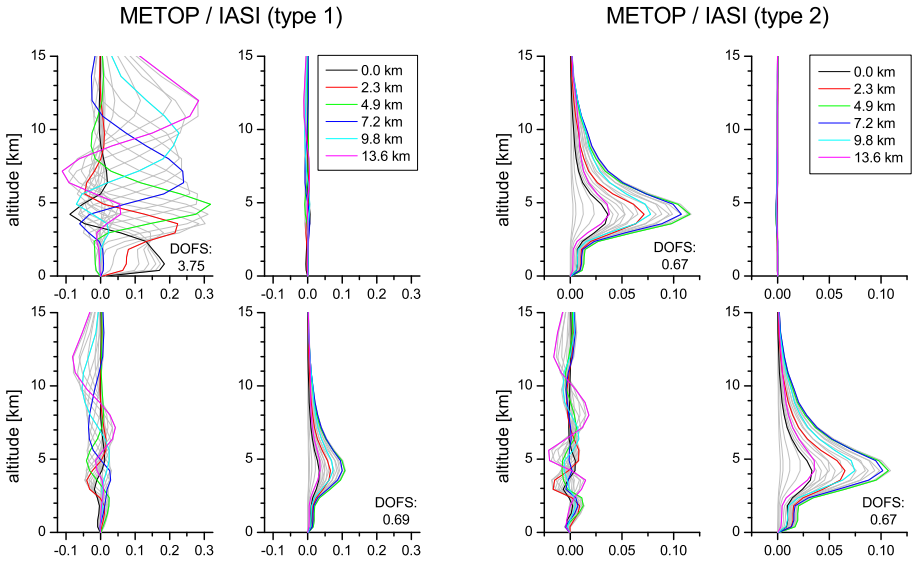

Figure 4. Same as Fig. 3 but for the {H_2O, δD}-proxy states as retrieved from METOP/IASI spectra measured over the subtropical ocean. For more details on the METOP/IASI proxy state kernels please refer to Schneider et al. (2012) and Wiegele et al. (2014).

AMTD
7, 6917–6969, 2014

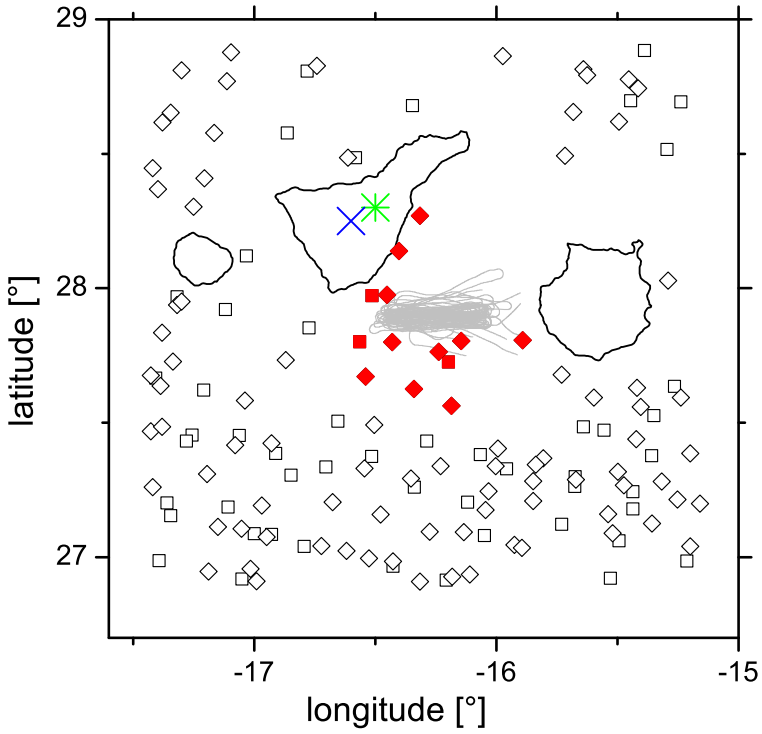

Figure 5. Site map indicating the location of the different instruments and ground pixels during the aircraft campaign on six days in July 2013. Green star: Izaña observatory (location of the first Picarro and the FTIR); blue star: Teide observatory (location of the second Picarro); gray lines: aircraft flight track during ISOWAT measurements; black squares and diamonds: cloud free ground pixels of IASI-A and -B, respectively, during the six aircraft flights ; red filled squares and diamonds: pixels that fulfill our coincidence criteria for IASI-A and -B, respectively.

AMTD
7, 6917–6969, 2014

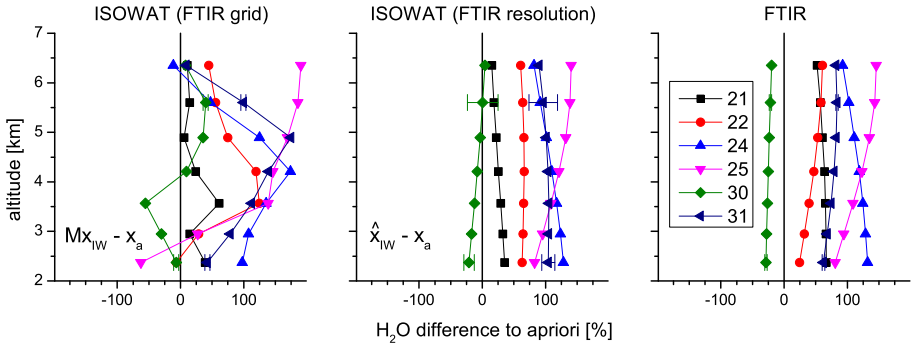

Figure 6. Comparison of ISOWAT and FTIR H_2O measurements. Shown are differences with respect to the apriori profiles. Left graph: ISOWAT data represented for the FTIR altitude grid; central graph: ISOWAT data convolved with the FTIR kernels, i.e., representative for the vertical resolution of the FTIR; right graph: FTIR data measured at the end of the morning when solar elevation is still $< 30^\circ$. Depicted are also lower and middle tropospheric error bars for day 130730 (dry conditions) and 130731 (humid conditions), which are hardly discernable, since the H_2O errors are only a few percent.

AMTD
7, 6917–6969, 2014

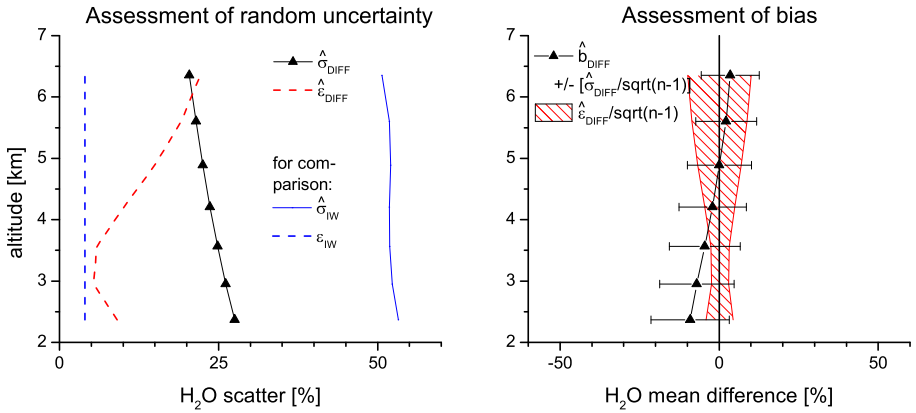

Figure 7. Left graph, assessment of the random uncertainty: black symbols: the FTIR-ISOWAT scatter ($\hat{\sigma}_{\mathrm{DIFF}}$ value according to Eq. 4). Red dashed line: the predicted scatter ($\hat{\epsilon}_{\mathrm{DIFF}}$ value according to Eq. 5). Blue solid line: the scatter in the convolved ISOWAT data ($\hat{\sigma}_{\mathrm{IW}}$ value according to Eq. 6). Blue dashed line: the uncertainty in the not convolved ISOWAT data (ϵ_{IW}). Right graph, assessment of the bias: black symbols and error bars: the FTIR-ISOWAT mean difference and standard error of the mean ($\hat{b}_{\mathrm{DIFF}}$ and $\hat{\sigma}_{\mathrm{DIFF}}/\sqrt{n-1}$ values according to Eqs. 3 and 4, respectively). Red area: the predicted uncertainty range (calculated as $\hat{\epsilon}_{\mathrm{DIFF}}/\sqrt{n-1}$).

AMTD
7, 6917–6969, 2014

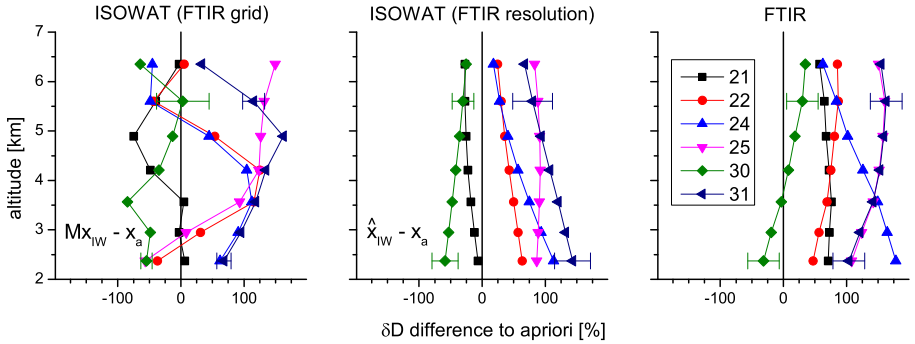

Figure 8. Same as Fig. 6 but for δD. Here the error bars are clearly discernable.

AMTD
7, 6917–6969, 2014

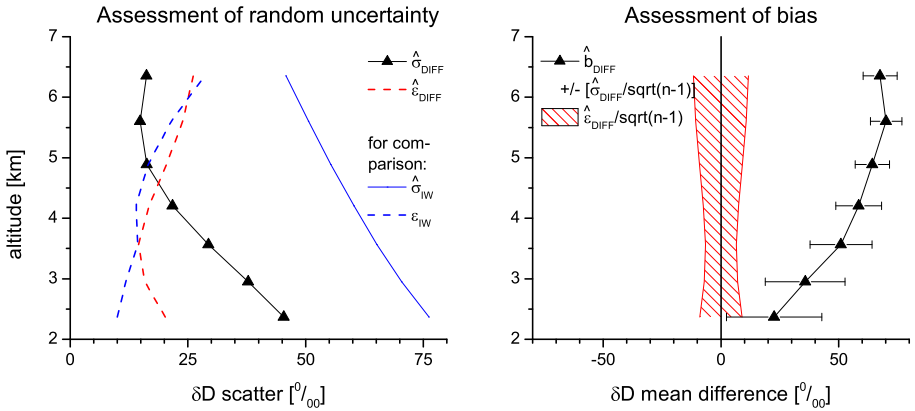

Figure 9. Same as Fig. 7 but for δD.

AMTD
7, 6917–6969, 2014

Empirical validation of δD remote sensing products

M. Schneider et al.

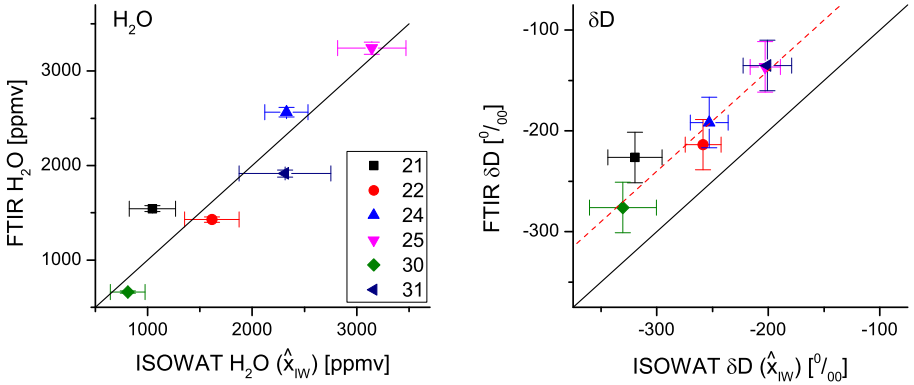

Figure 10. Correlation between ISOWAT data (smoothed with FTIR kernels) and FTIR data for 5 km altitude (left for H_2O and right for δD). Black line is the 1 : 1 diagonal and red dotted line is the 1 : 1 diagonal shifted by +60 ‰. Error bars represent the ISOWAT and FTIR uncertainty estimations. Please note that a large part of the uncertainty in the smoothed ISOWAT data is due to the fact that there are no ISOWAT measurements above the aircraft's ceiling altitude.

AMTD
7, 6917–6969, 2014

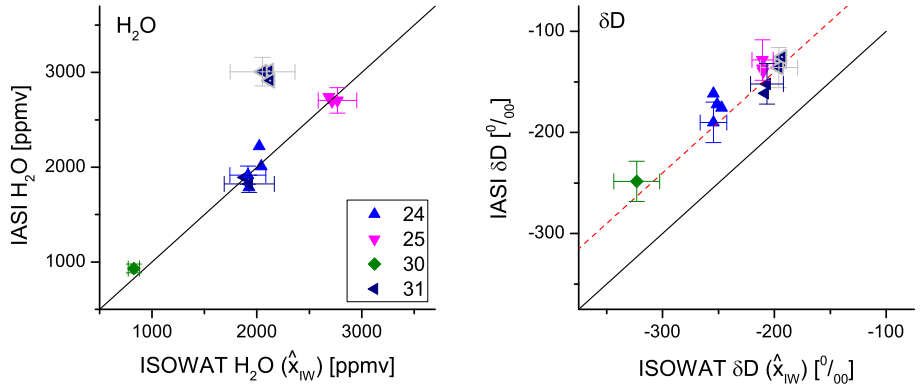

Figure 11. Same as Fig. 10 but for correlation between ISOWAT data (here smoothed with IASI kernels, i.e., this ISOWAT data are different to the ISOWAT data as depicted in Fig. 10) and IASI data for 5 km altitude. Three H_2O outliers on day 130731 (blue triangles) are marked by gray edges.

AMTD
7, 6917–6969, 2014

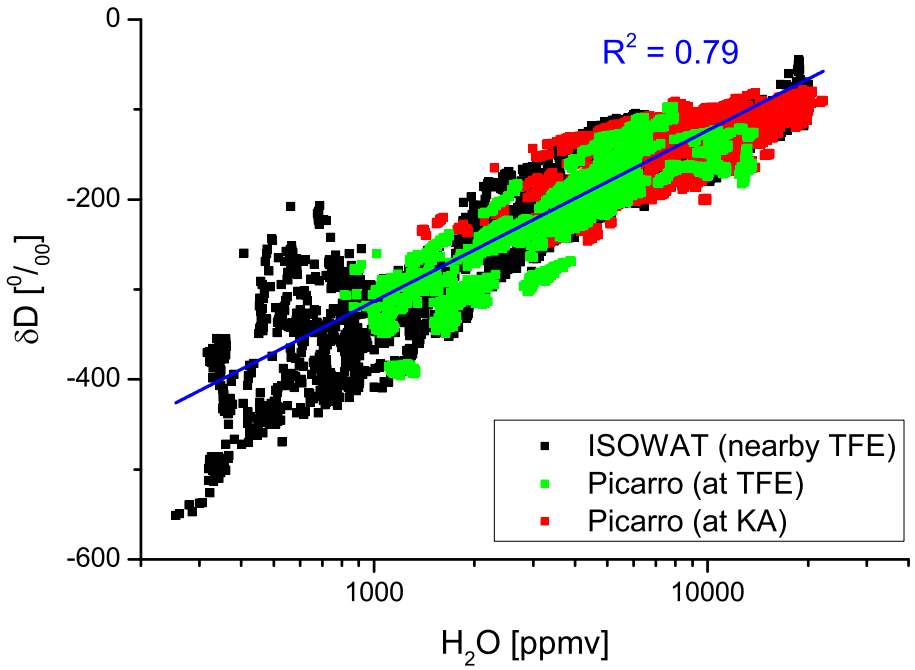

Figure 12. δD-vs.-H_2O plot using in-situ observations made from different platforms (aircraft/ISOWAT and surface/Picarro) and at different sites (mid-latitudes at Karlsruhe, KA, and subtropics at Tenerife, TFE). The blue solid line is the linear regression line as fitted to all the data points.

AMTD
7, 6917–6969, 2014

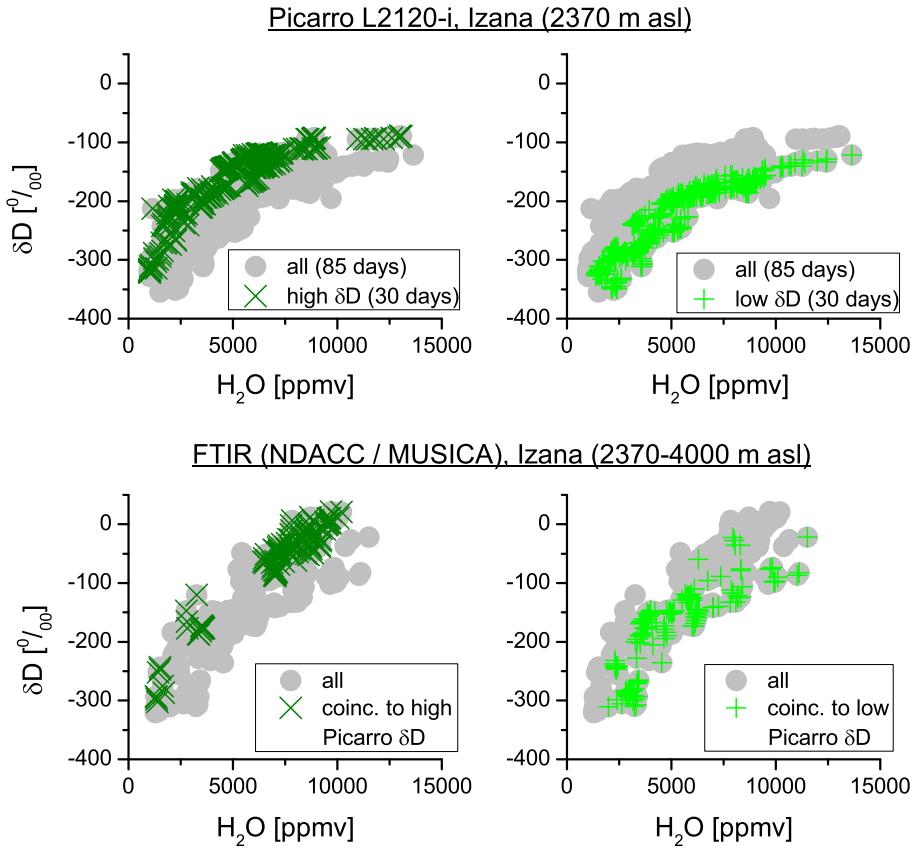

Figure 13. δD-vs.-H_2O plots for Picarro data measured at 06:00–08:00 UT at Izaña (2370 m a.s.l.) and for FTIR data measured during morning hours (solar elevation $< 30^\circ$) and representative for the altitudes between Izaña and $\approx$ 4000 m a.s.l.

AMTD
7, 6917–6969, 2014

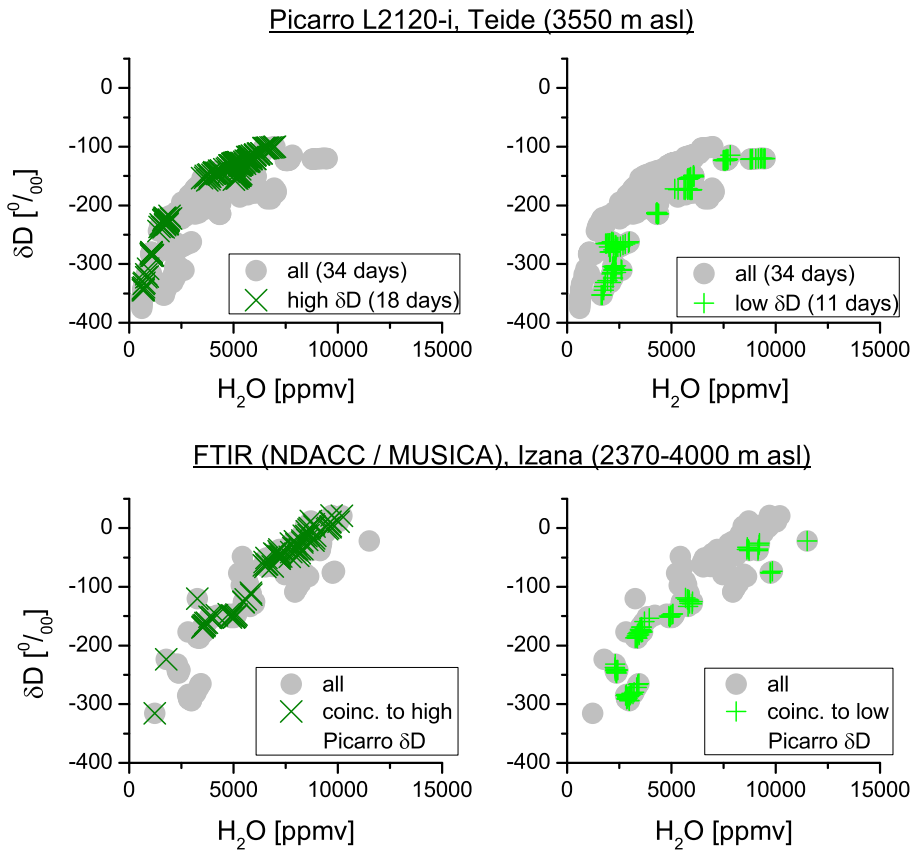

Figure 14. Same as Fig. 13 but for Picarro data measured at 06:00–08:00 UT at Teide (3550 m a.s.l.).

AMTD
7, 6917–6969, 2014

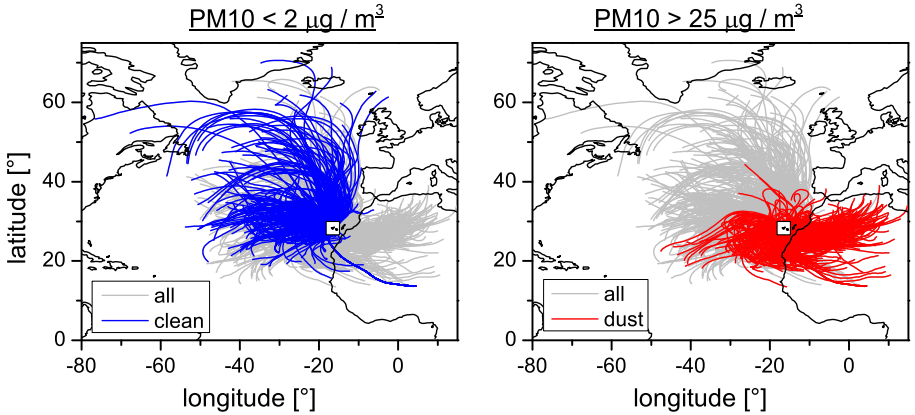

Figure 15. 72 h backward trajectories between May and October (2012 and 2013) for Izaña classified with respect to the PM_{10} value as measured in-situ at Izaña. Grey lines: all backward trajectories; blue lines: for $PM_{10} < 2\,\mu g\,m^{-3}$; red lines: for $PM_{10} > 25\,\mu g\,m^{-3}$.

AMTD
7, 6917–6969, 2014

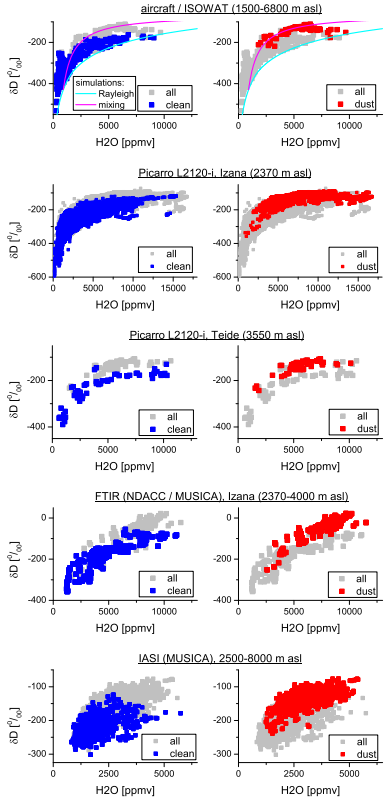

Figure 16. δD-vs.-H_2O plot observed from May to October at and close to Tenerife by different instruments. Gray dots: all data; blue dots: for airmass clearly not affected by the African continent; red dots: for airmass clearly affected by strong vertical mixing over the African continent. In addition the top panels show two simulated curves. Magenta line: mixing for $H_2O[1] = 25000$ ppmv; $\delta D[1] = -80$ ‰ and $H_2O[2] = 900$ ppmv; $\delta D[2] = -430$ ‰; cyan line: Rayleigh curve for initialisation with T = 25°C and RH = 80 %.

AMTD
7, 6917–6969, 2014

Empirical validation of δD remote sensing products

M. Schneider et al.

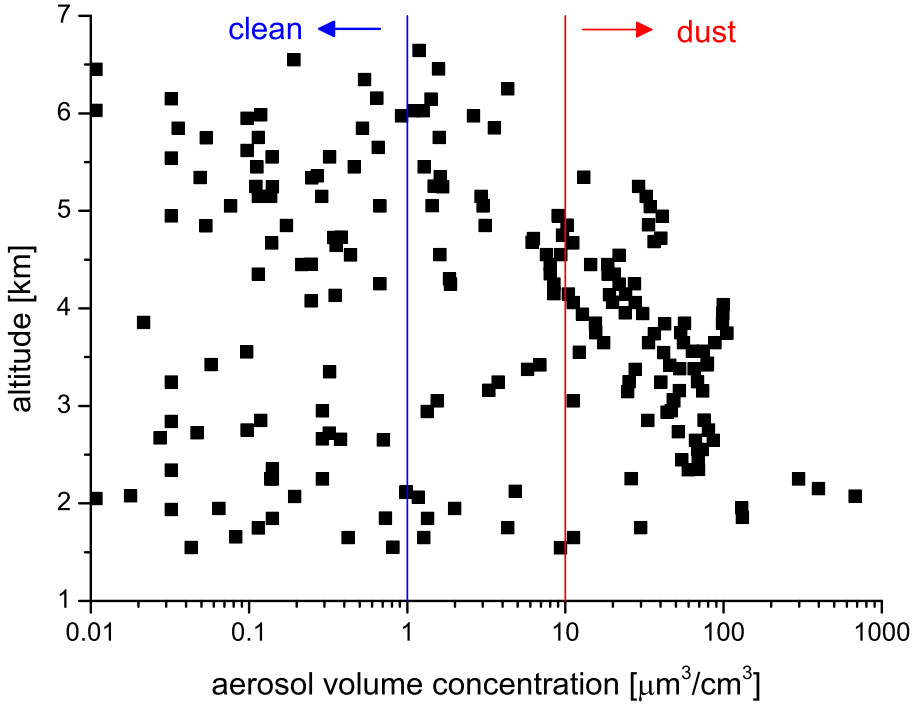

Figure A1. Vertical distribution of aerosol volume concentration (V_{10}) measured above the boundary layer during the six aircraft flights.

AMTD
7, 6917–6969, 2014

Empirical validation of δD remote sensing products

M. Schneider et al.

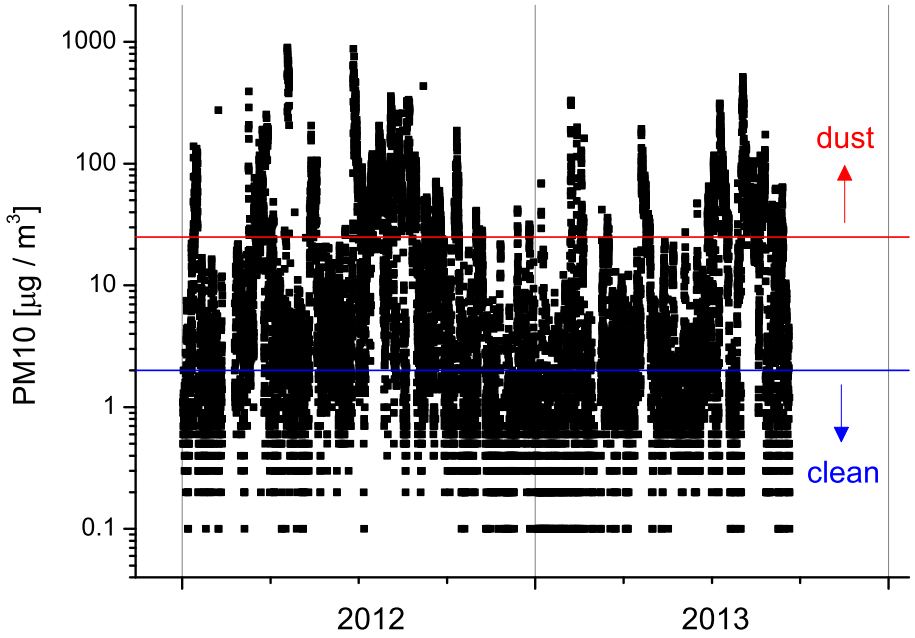

Figure A2. Time series of PM_{10} in-situ data as measured continuously at Izaña (2012–2013).

AMTD
7, 6917–6969, 2014

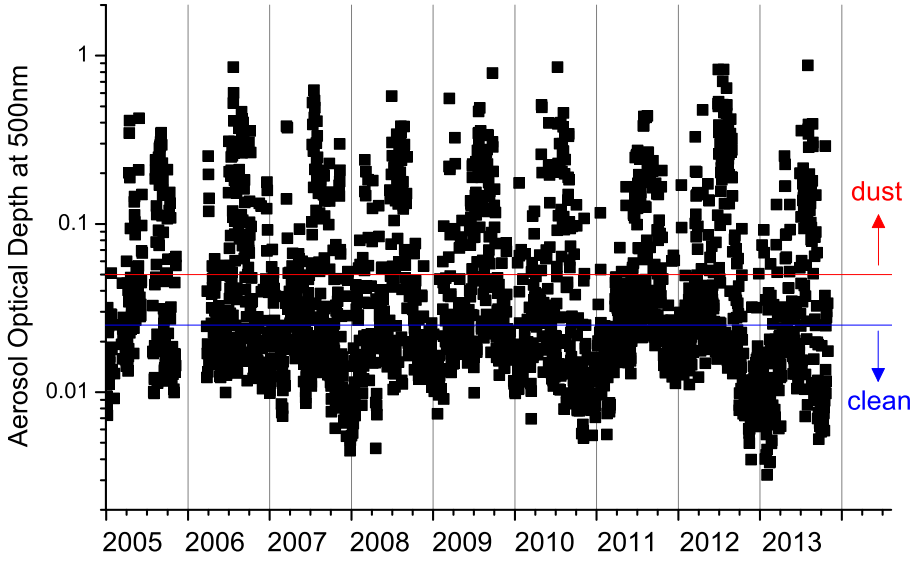

Figure A3. Time series of the AERONET aerosol optical depth at 500 nm reported for Izaña (2005–2012: level 2.0; 2013: level 1.5).

AMTD
7, 6917–6969, 2014